Monte Carlo model of ion mobility and diffusion for low and high electric fields

Scott Robertson and Zoltan Sternovsky

Department of Physics, University of Colorado, Boulder, Colorado 80309-0390

(Received 30 December 2002; published 29 April 2003)

A Monte Carlo method is described to model the mobility and diffusion of ions drifting in response to an electric field in a neutral gas. The model uses a collision frequency that is dependent upon the ion velocity and neutral gas thermal velocity. When implemented with a constant collision cross section for momentum transfer, the model gives a mobility that is constant for small electric fields (those giving a subsonic drift velocity) and that for larger fields falls inversely with the square root of the electric field. For argon ions drifting in argon, the model gives a close agreement with experimental data for the mobility for a wide range of electric fields when implemented with an energy-dependent cross section. For modeling of transverse diffusion, agreement with data is improved if the collisions are a combination of idealized charge-exchange collisions and hard-sphere collisions.

I. INTRODUCTION

The mobility of ions in weakly ionized plasma is often assumed to be constant, however, at higher field strengths it is a decreasing function of the electric field. The decrease begins at approximately the field strength that causes the drift velocity to exceed the thermal velocity of the neutral gas. In this work, a Monte Carlo model is described that gives good agreement with experimental data for the mobility of Ar^+ ions drifting in the parent gas for a wide range of electric field values. The computed mobility has the correct field dependence as a consequence of using an ion-neutral collision frequency that is a function of the ion velocity. In the development of this model, agreement with drift tube data for both mobility [1,2] and transverse diffusion [3,4] has been used as a guide. The transverse diffusion of drifting ions is more sensitively dependent upon the nature of the collisions than is the mobility. A combination of hard-sphere and idealized charge-exchange collisions is found to better reproduce data for transverse diffusion than either type of collision used alone. Combinations of types of collisions have previously been employed in modeling rf and dc discharges [5–12].

Plasma properties are often diagnosed by measuring the current-voltage characteristics of wire probes. For collisionless plasmas, the theory of probes is well developed, however, for collisional plasmas much less has been done in both theory and experiment. The frequently cited collisional probe theories [13,14] are based upon models in which the electron and ion motions are described by a constant mobility. The electric field, however, increases rapidly as the probe is approached and thus the ion mobility moves from the low-field regime to the high-field regime except for very small probe voltages. The use of a constant mobility limits these collisional probe theories to a relatively small range of voltage when ions are collected. A goal of the present work is to find a microscopic model for ion motion in plasmas that can be incorporated into computational models for ion collection by probes [15,16] and aerosol particles [17]. The model should also have applications in describing the sheaths in plasma processing.

In Sec. II below, the velocity dependence of the collision frequency is discussed and the theory of ion mobility is reviewed for both the low- and high-field cases. It is shown that these two limiting cases and the transition between them can be described by calculating the collision frequency using the mean velocity of collisions for ions drifting in a Maxwellian gas. In Sec. III, comparisons are made between computational models with fixed and velocity-dependent collision frequencies. The collision cross sections are assumed to be fixed or energy-dependent and the types of collisions are assumed to be hard sphere, charge exchange, or a combination of these. Computed values for mobility and transverse diffusions are compared with experimental data. A summary and conclusion are presented in Sec. IV.

II. THEORY

A. The collision model

The general expression for the collision frequency for a test ion of velocity $\vec{u}_i$ within the neutral parent gas is [18]

$$\nu(u_i) = n_n \int \sigma(|\vec{u}_i - \vec{u}_a|)|\vec{u}_i - \vec{u}_a|f(\vec{u}_a)d^3u_a, \quad (1)$$

where n_n is the neutral gas density, the integral is carried over the velocity distribution $f(\vec{u}_a)$ of the neutrals (assumed to be Maxwellian), and the collision cross section σ is written as a function of the relative velocities of the particles. The probability that an ion will have a collision in a differential time step dt is $\nu(u_i)\,dt$. This probability is independent of the choice of collision partner, because the integration removes the dependence upon $\vec{u}_a$. Thus, in the Monte Carlo model, it is not necessary to select the collision partner until after the decision to have a collision has been made.

The relative probability of a collision with an atom of given velocity $\vec{u}_a$ is determined by the dependence of the integrand upon $\vec{u}_a$. For collisions of electrons with atoms, the product of the cross section and relative velocity is often nearly a constant and may be taken out of the integrand. In this case, the distribution of collision partners is the same as the distribution of neutral gas atoms. In the case of charge-

exchange collisions of ions with atoms, there is a range of energies for which the cross section is nearly a constant. In this case it is appropriate to take the cross section out of the integrand and to use for it a single value at a representative collision energy. The remaining integrand is small where either $f(\vec{u}_a)$ is small or for values of $\vec{u}_a$ that are near to $\vec{u}_i$. The collision partners are therefore chosen using the weighting function

$$g(\vec{u}_i,\vec{u}_a) = |\vec{u}_i - \vec{u}_a| f(\vec{u}_a). \qquad (2)$$

If the collision partners were chosen from a simple Maxwellian (i.e., no multiplication by the relative velocity), collisions of atoms and ions of low relative velocity would be chosen at a too high rate and collisions of high relative velocity would be chosen at a too low rate. The consequences of alternate methods of choosing collision partners are discussed in the Appendix.

The choice of partner is implemented in the model by using the rejection method [19] applied to $g(\vec{u}_i,\vec{u}_a)$. The three components of a trial value of $\vec{u}_a$ are selected on the domain $(-3u_{th}, 3u_{th})$, where $u_{th} = (2T/m_i)^{1/2}$ is the thermal speed with the temperature T expressed in energy units and m_i is the mass of both the atoms and ions. The value of $g(\vec{u}_i,\vec{u}_a)$ is then compared to the value of $N_{\text{random}} \times \max[g(\vec{u}_i,\vec{u}_a)]$, and if the former is larger then the trial value of $\vec{u}_a$ is kept for the collision. Otherwise, the random selection of $\vec{u}_a$ is restarted. N_{random} is defined as a random number on the $(0,1)$ domain and $\max[g(\vec{u}_i,\vec{u}_a)]$ is the maximum value of the $g(\vec{u}_i,\vec{u}_a)$ function, which can be approximated as $(u_i + 0.5u_{th})$.

The integral in Eq. (1) is found approximately by taking the cross section outside the integral and defining $\nu(u_i) = n_n\sigma(w(u_i))w(u_i)$, where $w(u_i)$ is the mean relative velocity of collisions obtained from an integral over relative velocities. The mean velocity of collisions $w(u_i)$ for a test particle of velocity u_i moving among Maxwellian field particles is, after integration over solid angle [20],

$$w(u_i) = \frac{4}{u_{th}^3\sqrt{\pi}}\left[\int_0^{u_i}\frac{3u_i^2+u^2}{3u_i}u^2e^{-u^2/u_{th}^2}du\right.$$

$$+ \left.\int_{u_i}^{\infty}\frac{3u^2+u_i^2}{3u}u^2e^{-u^2/u_{th}^2}du\right]$$

$$\cong \left[\left(\frac{4u_{th}^2}{\pi}\right)^{a/2}+u_i^a\right]^{1/a}. \qquad (3)$$

The final expression, plotted in Fig. 1, is an approximation that is correct to within a few percent with $a=2$ and to within a few tenths of a percent with $a=2.14$. In the limit $u_i \rightarrow 0$, $w(u_i) \rightarrow (4/\pi)^{1/2}u_{th}$, and in the limit $u_i \gg u_{th}$, $w(u_i) \rightarrow u_i$. For subsonic ion velocity, the collision frequency is determined primarily by the mean speed of the neutral gas atoms and is only weakly dependent upon the test particle velocity. For supersonic ion velocities, the collision frequency is approximately $n_n\sigma(u_i)u_i$. The dependence of the collision frequency ν upon the ion velocity is
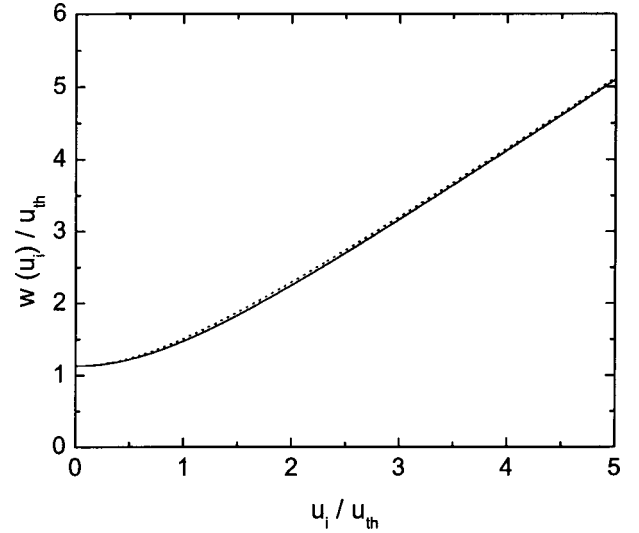
FIG. 1. The mean relative velocity between a test ion of speed u_{th} and the Maxwellian parent gas atoms. The solid line is from the integral in Eq. (3), the dotted line is the approximation with $a=2$. The velocities are normalized to the thermal speed u_i.

$$\nu(u_i) = \frac{w(u_i)}{\lambda_{\text{MFP}}} = \frac{\left[\left(\frac{4u_{th}^2}{\pi}\right)+u_i^2\right]^{1/2}}{\lambda_{\text{MFP}}}, \qquad (4)$$

where $\lambda_{\text{MFP}} = 1/n_n\sigma$ is the mean free path. This velocity-dependent collision frequency is used in the computational model.

The velocity-dependent collision frequency may be used in conjunction with the null collision method [21–23]. In this method, a collision frequency $\nu_{\max}$ is defined which is the largest value that is taken by $\nu(u_i)$. The probability of a collision per time step is initially defined as $\nu_{\max}dt$. If a collision is made, the true probability is calculated and the fraction $\nu(u_i)/\nu_{\max}$ of these collisions is completed. The collisions that are not made are referred to as null collisions. This method has the advantage that the possibly complicated expression for $\nu(u_i)$ is evaluated only for the fraction of collisions that are real collisions, e.g., not in every time step.

B. Mobility as a function of the electric field

In the fluid description of plasmas, the mobility is found from the momentum equation. The collisional drag is included by the term $-n_i m_i u_d \bar{\nu}_m$, where n_i is the ion density, $\bar{\nu}_m$ is the ensemble-averaged momentum transfer collision frequency, and u_d is the ion fluid drift velocity. Assuming a steady state, the fluid transport equation in one dimension is obtained as

$$\Gamma_i = n_i u_d = \mu_i n_i E - D_i \frac{dn_i}{dz}, \qquad (5)$$

where Γ_i is the ion flux, $\mu_i = q/m_i\bar{\nu}_m$ is the ion mobility, $D_i = T/m_i\bar{\nu}_m$ is the ion diffusivity, and q is the elementary charge. The electric field E is assumed to be uniform and aligned with the z axis. In general, D_i is a tensor quantity

with differing values parallel and transverse to the electric field. The momentum transfer collision frequency $\bar{\nu}_m$ is, in general, different from the frequency of computational collisions $\nu(u_i)$.

Often it is assumed that the mobility and diffusivity are constants and independent of the drift velocity. However, this is true only for drift velocities much smaller than the thermal speed. Wannier [24] identified three different regions for the mobility: (1) At small electric fields causing $u_d \ll u_{th}$, the collision frequency of the ions is a constant and the mobility is independent of the drift velocity. There is a generalized Einstein or Nernst-Townsend relation between mobility and diffusivity, $D_i/\mu_i = T^*/q$, where T^* is an effective temperature [25]. In the limit of small electric field, T^* is the temperature of the neutral gas. (2) At high electric fields causing $u_d \gg u_{th}$, the collision frequency increases linearly with the drift velocity and it is the mean free path that is approximately a constant. The collision frequency in this case can be expressed as $\bar{\nu}_m(u_d) = u_d/\lambda_{MFP}$. This relation placed in the momentum equation without a density gradient yields

$$u_d = \left(\frac{q\lambda_{MFP}}{m_i E}\right)^{1/2} E, \qquad (6)$$

where the mobility is now a decreasing function of the electric field intensity. (3) At intermediate electric fields, the drift velocity is of the order of the thermal speed. Laboratory measurements of the ion drift velocity show a very gradual change from a linear dependence upon E to a dependence upon $E^{1/2}$ as E is increased [26]. This transition occupies a large part of the parameter space and is treated in more detail in the following section.

C. An approximate expression for the drift velocity

Equation (4) that relates the collision frequency to the speed of the test ion is similar to an approximation suggested by Wannier [24], which uses a root-mean-square velocity to calculate the average collision frequency in the fluid approach

$$\bar{\nu}(u_d) = \frac{\left[\frac{3}{2}u_{th}^2 + u_d^2\right]^{1/2}}{\lambda_{MFP}}. \qquad (7)$$

This equation applies to the collision frequency averaged over all ion velocities rather than to the collision frequency of individual ions. It is thus a function of u_d rather than u_i. The drift velocity may be obtained by using Eq. (7) in the fluid momentum equation without a density gradient

$$u_d\left(\frac{3}{2}u_{th}^2 + u_d^2\right)^{1/2} = \frac{qE\lambda_{MFP}}{m_i}, \qquad (8)$$

which can be solved to find

$$u_d^*(E) = \left\{-\frac{3u_{th}^2}{4} + \frac{1}{2}\left[\left(\frac{3u_{th}^2}{2}\right)^2 + 4\left(\frac{qE}{m_i n_n \sigma_m}\right)^2\right]^{1/2}\right\}^{1/2}. \qquad (9)$$
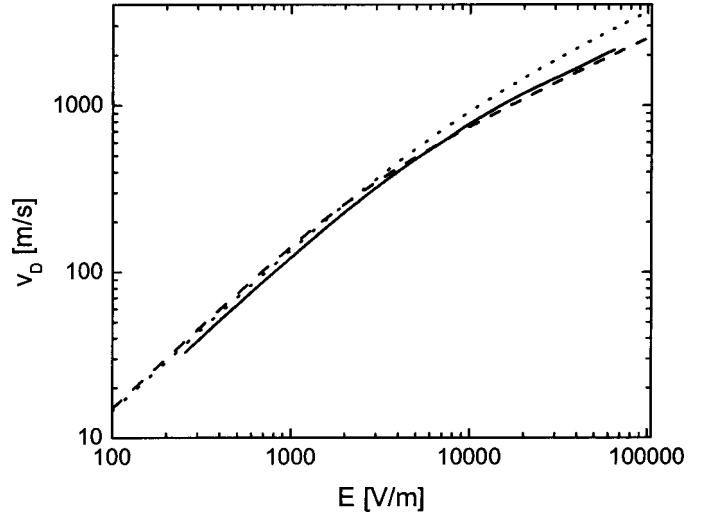
FIG. 2. The drift velocity as a function of electric field for Ar^+ ions in the parent gas at 1 Torr pressure and 300 K. The solid line is experimental data from Ref. [2], the dotted line is a fit by Frost (Ref. [27]), and the dashed line is from Eq. (9).

The drift velocity from Eq. (9) may be divided by the electric field to show that indeed the mobility is constant at low E, varies as $E^{-1/2}$ at high E, and that the transition occurs in the region where the drift velocity is comparable to the thermal velocity.

For the noble gas ions helium, neon, and argon, drifting in the parent gas, mobility measurements have been fit to a function of the form [27]

$$\mu_i(E) = \frac{\mu_{i,0}}{\left[1 + \frac{AE}{p}\right]^{1/2}}, \qquad (10)$$

where $\mu_{i,0}$ is the mobility extrapolated to zero electric field, p is the neutral gas pressure, and A is an adjustable constant. The drift velocity for argon based upon this formula with coefficients to fit experimental data [27] is shown in Fig. 2 along with the drift velocity from Eq. (9) evaluated using the cross section for momentum transfer [28] at ~ 1 eV of $\sigma_m = 1.15 \times 10^{-18}$ m². The close agreement shows that the velocity-dependent collision frequency $\bar{\nu}(u_d)$ gives accurate values for the mobility at low, intermediate, and high values of E when incorporated into the analytic model, Eq. (9). This suggests that a computational model based upon the collision frequency $\nu(u_i)$ should also be accurate. It is possible to include the energy dependence of the collision cross section, which has so far been ignored. This is discussed in more detail in the following section.

The relationship between the mobility and a constant charge-exchange mean free path has been discussed in some detail by Wannier [18,29] His analysis assumes an idealized charge exchange, in which the ion and atom exchange identity. He finds that the distribution function of drifting ions in the limit of a strong field is approximately a one-sided Maxwellian. The problem of relating the momentum transfer cross section to the charge-exchange cross section

has been discussed by Phelps [28]. This relationship depends upon the differential cross section for which there are only limited data, especially at low energies. The differential cross section [30] is peaked at 0° and 180° in the center of mass frame, which indicates that the commonly used hard-sphere model (isotropic in the center of mass frame) is a poor approximation. The small angle scattering has little effect on transport, and the backward scattering can be modeled as 180° backscatter. Phelps [28] suggests modeling the collisions as the sum of two processes: one in which there is a 180° backscatter and a second in which the scattering is isotropic. These are described by separate cross sections. The isotropic part of the cross section falls more rapidly with energy than the backscatter part, thus the backscatter is an increasing fraction of the total cross section as the collision energy is increased. The idealized charge exchange used by Wannier [18,29] is indistinguishable from 180° backscatter.

III. THE MONTE CARLO MODEL

A. Versions of the model

Computational models with increasing levels of complexity were compared in order to find the level necessary to give accurate values for mobility and diffusion for a wide range of E. The simplest models use dimensionless variables $q = m_i = u_{th} = E = 1$ and the results can easily be compared to analytic results. The more complicated models use values in SI units near to those in drift tube experiments. There are two types of collisions investigated: (1) The *identity switch*, which is the idealized charge-transfer collision, where the postcollision ion has the velocity of the neutral atom entering the collision, and (2) the *hard-sphere collision*, which is a random reorientation of the ion velocity vector in the center of mass frame. The neutral gas is either assumed cold or with a Maxwellian velocity distribution characterized by u_{th}. The collision partner is chosen either from a simple Maxwellian or from a velocity-weighted Maxwellian as described in Sec. II A. An earlier version of the model with infinitely massive neutrals was used to describe electron mobility and diffusion [31].

The motivation for developing the model is applications in which the electric field is not uniform. The model is tested, however, with uniform E, which allows the equations of motion to be integrated analytically. In the model, the motion of a test ion is followed in time steps. The decision to have a collision is made in either one of three ways. In the constant-ν versions, the probability of a collision per unit time has the same value for all ions. At each time step the collision probability is $\nu \, dt$. The time step is adjusted so that there are ~20 steps over the average collision time. This gives a small probability of a collision on each time step. In the constant-λ_{MFP} versions, the collision probability is ds/λ_{MFP}, where ds is the differential path length in time step dt. Again, the time step is adjusted for a small collision probability. In the variable-ν model, Eq. (4) is used to determine the collision frequency from the ion velocity and $\lambda_{MFP} = 1/n_n \sigma$. The mean free path is evaluated from either a constant cross section or an energy-dependent cross section evaluated at the mean velocity of collisions from Eq. (3).
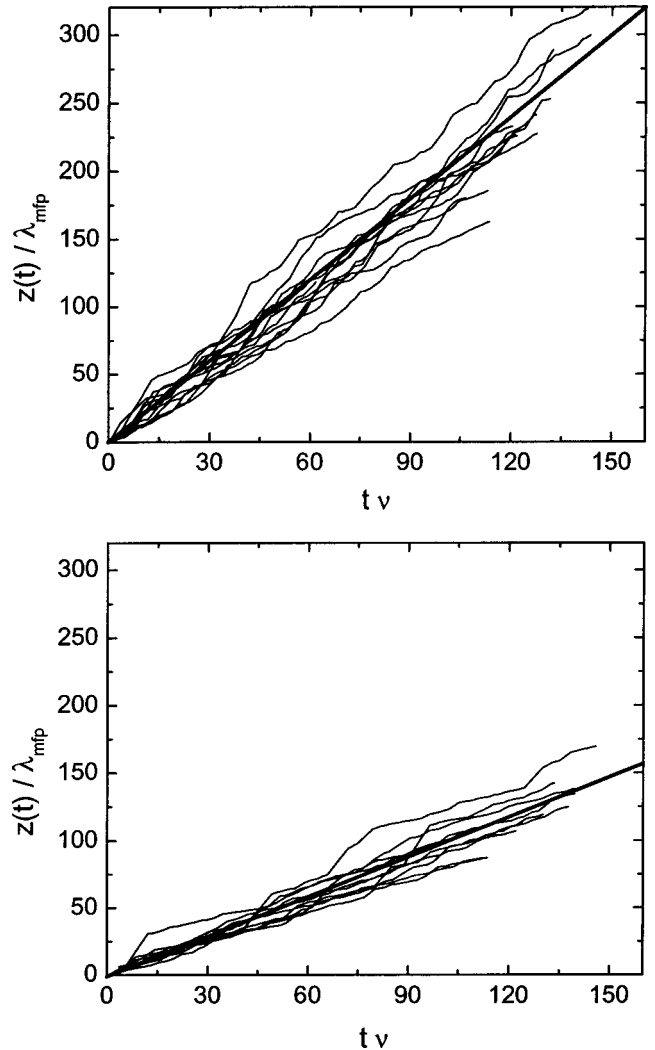
FIG. 3. Plots of the positions of ions along the z axis for the (a) hard-sphere and (b) identity-switch models. A constant collision frequency $\nu = 1$ and cold gas are assumed. The thick straight lines are linear regressions that determine the mean velocity. For clarity, only ten of the 128 trajectories are shown for each case.

In the time between collisions, the ion freely accelerates in an electric field along the z axis and moves along the other two axes at constant velocity. The number of particles followed is >256, and these are followed for >256 collision times. The statistical uncertainty in the diffusion values is about 2% and the uncertainty in the mobility is smaller.

B. Mobility in dimensionless variables

The first computations were done for the constant-ν case with dimensionless variables and $\nu = 1$. Figure 3 shows typical results for position as a function of time for the hard-sphere and identity-switch models, both for a cold gas. The linear regressions indicate that the drift velocities are 2.03 and 1.00, respectively. These are the expected values to within a few percent. The drift velocity in the hard-sphere model is twice as large as in the identity-switch case. This is because the identity-switch collisions are twice as effective removing the ion's momentum, thus $\bar{\nu}_m = 0.5$ for the hard-
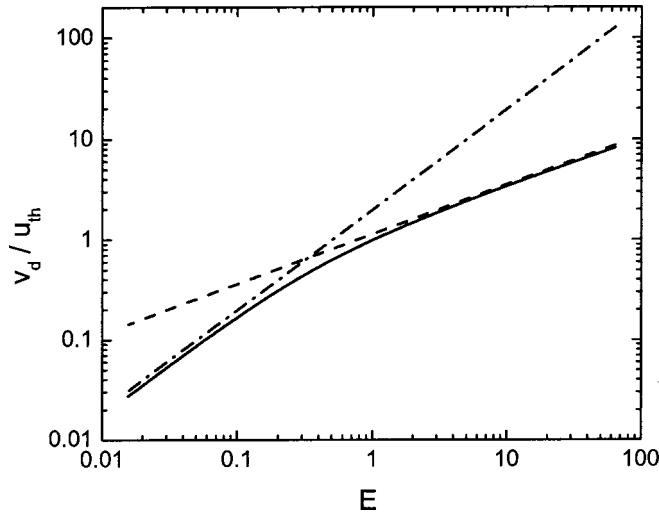
FIG. 4. The drift velocity as a function of the electric field for the constant-ν (dash-dotted line), constant-λ_{MFP} (dashed line), and variable-ν (solid line) models. The calculations are for dimensionless variables using the hard-sphere model and cold gas. The electric field is in units of one ion temperature drop over a mean free path. Using a Maxwellian distribution for the field particles $u_{th} = 1$ changes with the drift velocity by less than 2%.

sphere case and $\bar{\nu}_m = 1$ for identity switch. The spread in the $z(t)$ trajectories is a measure of the longitudinal diffusion. The deviations are smaller for the identity-switch case, because the difference in trajectories arises only from the randomness of the times of collisions. The constant-λ_{MFP} model with $\lambda_{MFP} = 1$ was also run for the two types of collisions. For the hard-sphere model, the drift velocity at $E = 1$ was 1.13, which is nearer to Wannier's theoretical value [24,32] of 1.147 $(qE\lambda_{MFP})^{1/2}$. The identity-switch collisions gave 0.785 for the drift speed at the same conditions, which is nearer to the value of $(2/\pi)^{1/2}$ derived by Wannier [18].

The scaling of the drift velocity with electric field was investigated for a wide range of E using cold gas with both the constant-ν, and the constant-λ_{MFP} models, Fig. 4. Linear regressions show scaling in the constant-ν case with the 1.000 power of E and in the constant-λ_{MFP} case with the 0.499 power of E. The variable collision frequency was implemented by using Eq. (4) with $\lambda_{MFP} = 1$. Collisions were with Maxwellian gas with $u_{th} = 1$. The dependence of the drift velocity upon the electric field, the solid line in Fig. 4, shows a smooth transition from the constant-ν case at low values of E to the constant-λ_{MFP} case at high values.

C. Modeling mobility of Ar$^+$ in Ar gas

Argon is one of the most widely studied gases and there are many measurements of mobility, diffusion, and collision cross sections. The computations were repeated for Ar$^+$ ions using variables in SI units. The neutral Ar gas was modeled with $n_n = 3.535 \times 10^{22}$ m^{-3} and 300 K temperature giving $u_{th} = 352$ m/s. Three collision cross-section models were used. The first is a constant momentum transfer cross section, $\sigma_m = 1.15 \times 10^{-18}$ m^2. The second is an energy-dependent cross section [28]

$$\sigma_m(\epsilon) = 1.15 \times 10^{-18} \varepsilon^{-0.1}(1 + 0.015/\varepsilon)^{0.6}, \quad (11)$$

with the collision energy ε expressed in eV. This cross section varies approximately as $\varepsilon^{-0.1}$ for $\varepsilon \geqslant 0.015$ eV. For these energies, the removal of the cross section from the integrand in Eq. (1) is justified and Eq. (2) is a good approximation.

The third cross section is a net cross section that is the sum of two parts,

$$\sigma_{net}(\varepsilon) = \sigma_b(\varepsilon) + \sigma_i(\varepsilon), \quad (12)$$

where $\sigma_b(\varepsilon)$ is the cross section for 180° backscatter in the center of mass frame (idealized charge exchange) and $\sigma_i(\varepsilon)$ is the cross section for isotropic scattering [28] (hard-sphere collision). Data for the differential scattering cross section has been used to deduce the isotropic part of the collision cross section [28]:

$$\sigma_i(\varepsilon) = \frac{2 \times 10^{-19}}{\varepsilon^{0.5}(1 + \varepsilon)} + \frac{3 \times 10^{-19}\varepsilon}{(1 + \varepsilon/3)^{2.3}}. \quad (13)$$

The backscatter cross section $\sigma_b(\varepsilon)$ can be deduced by subtracting the isotropic part of the cross section from the cross section for momentum transfer, taking into consideration the fact that backscatter collisions remove twice the momentum, on average, as the isotropic collisions. The momentum transfer cross section can be expressed as $\sigma_m(\varepsilon) = 2\sigma_b(\varepsilon) + \sigma_i(\varepsilon)$. The backscatter cross section is then $\sigma_b(\varepsilon) = [\sigma_m(\varepsilon) - \sigma_i(\varepsilon)]/2$ and $\sigma_{net}(\varepsilon) = [\sigma_m(\varepsilon) + \sigma_i(\varepsilon)]/2$. In the model with the net cross section, the value of $\sigma_{net}(\varepsilon)$ is used to make the decision for a collision, and the comparison of a random number to $\sigma_i(\varepsilon)/\sigma_{net}(\varepsilon)$ is used to select either a hard-sphere collision or a backscatter collision.

The collision energy is calculated from the mean velocity of collisions $w(u_i)$ according to Eq. (3). The smallest collision energy is then approximately the thermal energy and Eq. (12) is never evaluated at energies below 0.03 eV where the cross section begins to diverge. The calculated drift velocities obtained with the different cross section models are shown in Fig. 5 and listed in Table I. Measured drift velocities from two experiments [1,2] are also listed. The drift velocities obtained with the energy-dependent cross sections are in good agreement with the data, but the constant cross section gives values that are too high at low electric field. This is partially a consequence of using a fixed value for the cross section that is inappropriate for low velocity collisions. In most of the calculations for Fig. 5 and Table I, the collision partner has been selected from a simple Maxwellian. In column 5 of Table I, a second number is given which is the drift velocity calculated for the energy-dependent cross section $\sigma_m(\varepsilon)$ using collision partners selected from the velocity-weighted Maxwellian. The velocity-weighted selection reduces the drift velocities because of the favored selection of collision partners with velocities in the opposite direction from the ion. This occurs because $|\vec{u}_i - \vec{u}_a|$ is greater for these partners. The difference in drift velocities is smaller for high drift velocity, where the relative important of u_a is smallest.
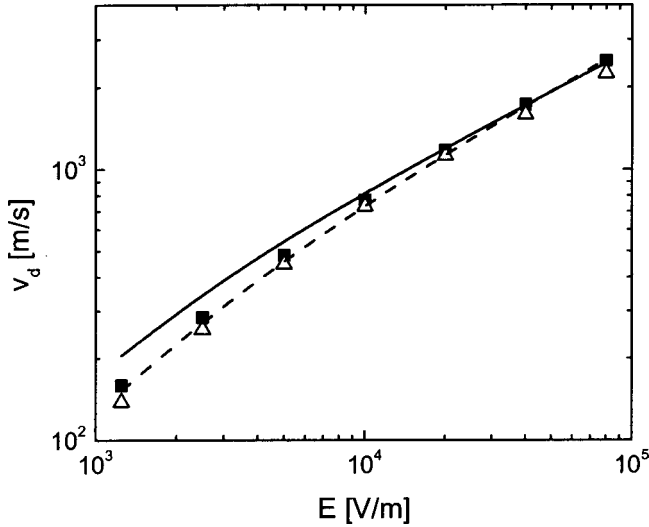
FIG. 5. A comparison of the experimental drift velocity from Hornbeck [1] (solid squares) and Beaty [2] (open triangles) with mobilities computed using a constant cross section (solid line), and the energy-dependent net cross section in Eq. (11) (dashed line). See also Table I.

The model was not run for argon with a constant collision frequency or mean free path. It is clear from inspection of Fig. 3 that mobilities calculated in either of these ways will have significant error at either high or low values of electric field. Experimental mobilities for argon for a wide range of E have been reproduced in the Monte Carlo model of Nanbu and Kitatani [33], who used cross sections with adjustable cutoffs. The model presented here has no adjustable parameters.

D. Transverse diffusion

Ion diffusion with zero electric field was investigated for Maxwellian field particles using the constant-ν model with

TABLE I. A comparison of measured drift velocities for argon with velocities from four computational models using different collision and cross-section models. The collision frequency is given by Eq. (4). The second number in the fifth column lists drift velocities where the velocity-weighted collision partner selection was applied. The listed experimental values were obtained from the references by interpolation. The statistical uncertainties in the computational values are below 2%.

	Drift velocities [m/s]			
E (V/m)	Hornbeck [1]	Beaty [2]	From σ_m	From $\sigma_m(\varepsilon)$	From $\sigma_b(\varepsilon)+\sigma_i(\varepsilon)$
1250	159	138	205	151/131	152
2500	284	256	346	278/251	273
5000	481	447	547	474/445	461
10 000	769	732	817	756/729	735
20 000	1173	1125	1196	1163/1139	1132
40 000	1730	1592	1719	1737/1711	1706
80 000	2502	2252	2451	2583/2543	2529

TABLE II. The effective temperatures T^* from transverse diffusion obtained from experiments (column 2), from computational models with idealized charge-exchange collisions (column 3), and from hard-sphere collisions (column 4). The last column is from a model using a mixture of hard-sphere and idealized charge exchange. The first number is for collision partners chosen from the simple Maxwellian and the second number is for the velocity-weighted Maxwellian.

	$T^*=D_T/\mu$ (meV)			
E (V/m)	Sejkora et al. [3]	Identity switch σ_m	Hard sphere σ_m	Mixture $\sigma_b(\varepsilon)+\sigma_i(\varepsilon)$
1250	28	24/25	27/28	24/29
2500	31	24/26	33/35	25/29
5000	38	26/25	49/51	30/33
10 000	48	26/26	83/86	37/39

dimensionless variables and hard-sphere collisions. The computational collision frequency was set to $\nu=2$ so that $\bar{\nu}_m=1$. The diffusivity was determined from a linear regression using the relation $\langle r^2\rangle=6D_i t$, where $\langle r^2\rangle$ is the root-mean square of the radial distance from the origin. The measured slopes for five repetitions of the model gave an average of 3.01 with a standard error of ± 0.09 indicating $D_i=0.50\pm 0.02$. This is near to the expected diffusivity, $D_i=T/m_i\bar{\nu}_m=0.5$, where in the dimensionless units $T=0.5$ and $u_{th}=m_i=1$. Sampling of the atom and ion velocities verified that the mean-squared velocity $\langle u^2\rangle=1.5$ is for both (see also the Appendix).

The diffusion of argon ions transverse to an electric field, D_T, was also investigated, because it is a sensitive indicator of angular scattering. A linear regression was used to find D_T from the relation $\langle r^2\rangle=4D_T t$. Experimental values for the effective temperature T^* are available [3,4], thus D_T was divided by the mobility (obtained from u_d/E) to find T^*. A comparison is given in Table II for different collision types and different techniques for the selection of collision partners. For identity-switch collisions, the temperature of the neutral gas determines the transverse motion, and the transverse diffusivity does not change with E. If there is a momentum transfer, as in hard-sphere collisions, then D_T and T^* are increasing functions of E. These two collision models were run with warm gas, collision partners chosen from a simple Maxwellian, and constant collision cross section. The experimental data falls between the two cases, indicating that the argon ion-atom collisions have a momentum transfer between that of hard-sphere collisions and idealized charge exchange. The effective temperature from the model is closer to the experimental values when mixed collisions with their corresponding energy-dependent cross section are used. The values are consistently low by more than the experimental error, suggesting that the collisions have a larger isotropic component. The energy-dependent cross sections result in about 40% of the collisions, being idealized charge ex-
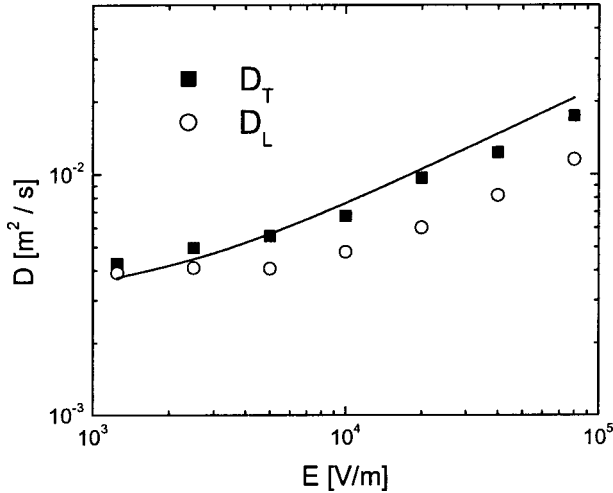
FIG. 6. Diffusivities D_L (squares) and D_T (open circles) for argon ions drifting in argon. The solid line is D^*.

change, at $E = 1250$ V/m and about 65% at $E = 10\,000$ V/m. Selecting the collision partner from a velocity-weighted Maxwellian, the second numbers in Table II, increases slightly the effective temperature obtained with hard-sphere collisions.

E. Longitudinal diffusion with hard-sphere collisions

For argon ions in argon, longitudinal diffusion is too small for accurate experimental measurements to be made. The model was therefore run with only hard-sphere collisions, and the results were compared with the theoretical results for the same kind of collisions. The longitudinal diffusion was found from the deviations of individual trajectories from the mean trajectory. The squares of these deviations increase as $2D_L t$. Both D_L and D_T from this model are shown in Fig. 6 for a range of electric fields spanning the low- and high-field cases. At the smallest value of E investigated, $D_T/\mu_i = 0.025$ eV and $D_L/\mu_i = 0.023$ eV which are nearer to the expected value of 0.026 eV. Diffusivities with a constant mean free path [34] can be written as $\langle u \rangle \lambda_{\text{MFP}}/3$ in the limit of zero electric field. If the mean speed $\langle u \rangle$ is interpreted as $w(u_d)$, a characteristic diffusivity $D^* = w(u_d)\lambda_{\text{MFP}}/3$ can be defined for convenience that has approximately the correct scaling with E. The computed values of D_T are nearer to D^* for low E and fall to $0.88\,D^*$ at the highest E investigated. The longitudinal diffusivity is nearer to D^* at low electric fields but falls more rapidly approaching $0.5\,D^*$ at high field. Skullerud [35] points out that for longitudinal motion, the ions that are in front of a group are moving the fastest, and thus have the highest collision frequency. This tends to slow them causing a bunching effect that reduces the longitudinal spread. Skullerud [35] has investigated the high-field case with a Monte Carlo code and finds $D_T = 0.32(qE\lambda^3_{\text{MFP}}/m_i)^{1/2}$ and $D_L = 0.22(qE\lambda^3_{\text{MFP}}/m_i)^{1/2}$. The values found here at the highest fields are approximately

the same as Skullerud's D_T and about 10% lower than his D_L.

The mean energies of the ions were also computed and found to be 0.87 ± 0.05 of the value suggested by Heimerl *et al.* [36],

$$\frac{1}{2}m_i\langle u^2 \rangle = \frac{\pi}{4}m_i u_d^2 + \frac{3}{2}T, \tag{14}$$

throughout the range of E investigated. This formula is similar to one given earlier for the constant-ν case by Wannier [24], in which the first term on the right has a coefficient of unity rather than $\pi/4$.

IV. CONCLUSIONS

A Monte Carlo model in which the collision frequency is calculated from the mean velocity of collisions has been found to accurately reproduce the electric field dependence of the mobility. The drift velocities scale linearly with E at low electric fields and with $E^{1/2}$ at high electric fields. The data in Table I compare the drift velocities that are obtained with models of differing complexity. Comparison of column 4 with constant cross section and column 5 with an energy-dependent cross section show that including the energy dependence significantly improves agreement with drift tube data at the smaller values of drift velocity. Note, however, that the constant value of the cross section used for column 4 was selected to give good agreement at high drift velocity. If a larger cross section had been used, the agreement would have been better at low drift velocity and poorer at high drift velocity. Comparison of the drift velocities in column 5 for hard-sphere collisions and column 6 for a mixture of collision types shows that the more complex model does not significantly change the drift velocity. Thus if reproducing mobility is the only concern, there is a little to be gained from using a mixture of collision types. On the other hand, the drift velocity is significantly changed (second number in column 5) if collision partners are chosen correctly using the velocity-weighted Maxwellian. The computed drift velocities in this case are nearer to the drift tube data of Beaty [2]:

Calculated transverse diffusivities are too large when a hard-sphere collision model is used and too small when an idealized charge-exchange model is used. Diffusivities nearer to the experimental values are obtained by using a mixture of hard-sphere and idealized charge-exchange collisions calculated from separate energy-dependent cross sections. The data in Table II suggest that the fraction of the cross section that is isotropic is greater than indicated by the cross section in Eq. (13). The selection of collision partners using a velocity-weighted Maxwellian increases slightly the diffusivity by increasing the population of high velocity ions.

APPENDIX: CHOICE OF COLLISION PARTNERS

It is expected from statistical mechanics that in the absence of an electric field, the ion distribution will become Maxwellian as a consequence of collisions with atoms that have a Maxwellian distribution. The adoption of a collision frequency that increases with velocity, Eq. (4), reduces the lifetime of the suprathermal ions. If the ions created by collisions initially have a Maxwellian distribution, then the higher collision frequency of the faster ions will result in their being preferentially lost and are thus under-represented in the distribution. This effect is illustrated in Fig. 7(a) where the ion distribution functions obtained with two collision models are compared with a Maxwellian distribution. Both distributions were obtained by following one ion for $>10^5$ collisions and sampling the velocity at equally spaced time intervals longer than several collision times. In both models the collision frequency is velocity dependent and is given by Eq. (4). The measured distribution is nearly Maxwellian when the collision partners are chosen using the velocity-weighted Maxwellian. The measured distribution has too few high energy particles and too many low energy particles when the collision partners are chosen from the simple Maxwellian. This is also indicated by the second moments of the distributions. The root-mean-squared velocities in the two cases are 1.51 and 1.29, respectively. If a constant collision frequency is used and the collision partners are chosen from the velocity-weighted Maxwellian, the observed distribution is shifted toward higher velocities, and the root-mean-squared value is 1.74. This indicates that choosing collision partners from the velocity-weighted Maxwellian "corrects" the effect of the velocity-dependent collision frequency by
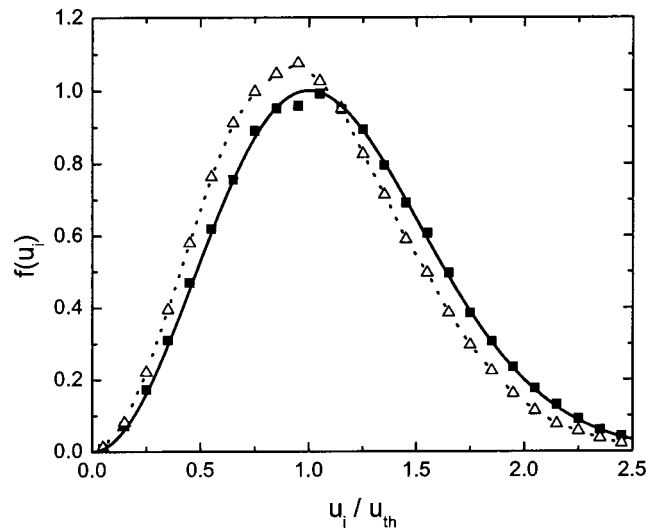
FIG. 7. The ion velocity distribution obtained from the computational model using $E=0$ and dimensionless units. The solid squares are the ion distribution obtained from the variable-ν case with selection of collision partners from the velocity-weighted Maxwellian. The open triangles are from the variable-ν case with partners selected from the simple Maxwellian. The solid line is a Maxwellian distribution. The distributions are normalized to the same number of ions and the velocity is normalized to the thermal velocity.

generating the high velocity ions at a greater rate. As discussed in Sec. III C, the effect of choosing collision partners with the velocity weighting is to reduce the mobility at low values of E and to slightly increase the diffusivity at all values of E.

[1] J. A. Hornbeck, Phys. Rev. **84**, 615 (1951).

[2] E. C. Beaty, in *Ionization Phenomena in Gases*, Proceedings of Fifth International Conference, Munich (North-Holland, Amsterdam, 1961) Vol. 1, p. 83, quoted in H. W. Ellis, R. Y. Pai, E. W. McDaniel, E. A. Mason, and L. A. Viehland, At. Data Nucl. Data Tables **17**, 177 (1976).

[3] G. Sejkora, P. Girstmair, H. C. Bryant, and T. D. Märk, Phys. Rev. A **29**, 3379 (1984).

[4] R. N. Varney, H. Helm, E. Alge, H. Störi, and W. Lindinger, J. Phys. B **14**, 1695 (1981).

[5] B. E. Thompson, H. H. Sawin, and D. A. Fisher, J. Appl. Phys. **63**, 2242 (1988).

[6] A. C. Dexter, T. Farrell, and M. I. Lees, J. Phys. D **22**, 413 (1989).

[7] J. Liu, G. L. Huppert, and H. H. Sawin, J. Appl. Phys. **68**, 3916 (1990).

[8] R. T. Farouki, S. Hamaguchi, and M. Dalvie, Phys. Rev. A **44**, 2664 (1991).

[9] A. Manenschijn and W. J. Goedheer, J. Appl. Phys. **69**, 2923 (1991).

[10] P. W. May, D. Field, and D. F. Klemperer, J. Appl. Phys. **71**, 3721 (1992).

[11] D. Wang, T. Ma, and X. Deng, J. Appl. Phys. **75**, 1335 (1994).

[12] A. Bogaerts and R. Gijbels, IEEE Trans. Plasma Sci. **27**, 1406 (1999).

[13] C. H. Su and S. H. Lam, Phys. Fluids **6**, 1479 (1963).

[14] I. M. Cohen, Phys. Fluids **6**, 1492 (1963).

[15] Z. Sternovsky and S. Robertson, Appl. Phys. Lett. **81**, 1961 (2002).

[16] Z. Sternovsky, S. Robertson, and M. Lampe, Phys. Plasmas **10**, 300 (2003).

[17] M. Lampe, V. Gavrishchaka, G. Ganguli, and G. Joyce, Phys. Rev. Lett. **86**, 5278 (2001).

[18] G. H. Wannier, *Statistical Physics* (Dover, New York, 1987), Chaps. 18 and 21.

[19] D. E. Knuth, *The Art of Computer Programming* (Addison-Wesley, Reading, MA, 1969), Vol. 2.

[20] L. B. Loeb, *The Kinetic Theory of Gases* 3rd ed., (Dover Publications, New York, 1961), p. 96.

[21] S. L. Lin and J. N. Bardsley, J. Chem. Phys. **66**, 435 (1977).

[22] J. P. Boeuf and E. Marode, J. Phys. D **15**, 2169 (1982).

[23] C. K. Birdsall, IEEE Trans. Plasma Sci. **19**, 65 (1991).

[24] G. H. Wannier, Bell Syst. Tech. J. **32**, 170 (1953), Eqs. (92), (100), and (166).

[25] E. W. McDaniel, J. B. A. Mitchell, and M. E. Rudd, *Atomic Collisions: Heavy Particle Projectiles* (Wiley, New York, 1993), Chap. 7.

[26] E. W. McDaniel, *Collision Phenomena in Ionized Gases* (Wiley, New York, 1964), Chap. 9.

[27] L. S. Frost, Phys. Rev. **105**, 354 (1957).

[28] A. V. Phelps, J. Appl. Phys. **76**, 750 (1994).

[29] G. H. Wannier, Phys. Rev. **83**, 281 (1951).

[30] M. L. Vestal, C. R. Blakley, and J. H. Futrell, Phys. Rev. A **17**, 1337 (1978).

[31] Q. Quraishi and S. Robertson, Phys. Rev. E **62**, 1405 (2000).

[32] J. A. Hornbeck and G. H. Wannier, Phys. Rev. **82**, 458 (1951).

[33] K. Nanbu and Y. Kitatani, J. Phys. D **28**, 324 (1995).

[34] I. P. Shkarofsky, T. W. Johnston, and M. P. Bachynski, *The Particle Kinetics of Plasmas* (Addison-Wesley, Reading, MA, 1966), p. 128.

[35] H. R. Skullerud, J. Phys. B: Atom Molec. Phys. **6**, 728 (1973).

[36] J. M. Heimerl, R. Johnsen, and M. A. Biondi, J. Chem. Phys. **51**, 5041 (1969).